Hindawi
Advances in Materials Science and Engineering
Volume 2022, Article ID 2748908, 9 pages
https://doi.org/10.1155/2022/2748908

Research Article

Synthesis and Characterization of Iron Doped Titanium Dioxide (Fe: TiO_2) Nanoprecipitate at Different pH Values for Applications of Self-Cleaning Materials

Tizazu Abza,[1] Abel Saka,[2] Jule Leta Tesfaye,[2,3] Lamessa Gudata,[2] N. Nagaprasad,[4] and Ramaswamy Krishnaraj[3,5]

[1]*Hawassa University, College of Natural and Computational Sciences, Physics Department, Hawassa, Ethiopia*
[2]*Dambi Dollo University, College of Natural and Computational Science, Department of Physics, Ethiopia*
[3]*Centre for Excellence-Indigenous Knowledge, Innovative Technology Transfer and Entrepreneurship, Dambi Dollo University, Ethiopia*
[4]*Department of Mechanical Engineering, ULTRA College of Engineering and Technology, Madurai - 625 104, Tamilnadu, India*
[5]*Department of Mechanical Engineering, College of Engineering, Dambi Dollo University, Ethiopia*

Correspondence should be addressed to Abel Saka; latiyejesus@gmail.com, Jule Leta Tesfaye; laterajule@gmail.com, and Ramaswamy Krishnaraj; prof.dr.krishnaraj@dadu.edu.et

Received 1 May 2022; Revised 27 May 2022; Accepted 10 June 2022; Published 8 July 2022

Academic Editor: Pudhupalayam Muthukutti Gopal

Fe:TiO_2 nano particles were deposited through sol-gel techniques, and the influence of pH values on structural, morphological, optical, and photoluminescence spectral behaviors was studied. Iron doped titanium dioxide nanopowders were analyzed using XRD, SEM, UV–ViS, and PL. Nano crystallized samples of titanium dioxide (72 nm, 77 nm, 78 nm, and 83 nm) were gained from X-Ray diffraction data and showed that there was the creation of unalloyed anatase and ructile segment with tetragonal configuration. The average crystal size was 77.5 nm. pH values provide the alteration of segments from anatase to ructile. The crystal size of prepared iron doped titanium dioxide nanoparticles was greater than before as pH value rises from 2 to 6 while FWHM and scrap sizes declined. Homogeneously disseminated cylindrical forms of iron doped titanium dioxide nanoparticles were perceived from scanning electron microscope graphics and rises in size with growing pH values from 2 to 6 in an acidic medium. Extremely translucent nanopowders are witnessed in the observable region by visible and redshifts near advanced wavelengths with rising pH values because of an increase in the size of particles from XRD data and SEM micrographs. The band gap of energy produced by nano concentrates was reduced with growing pH values that resemble the redshift of optical absorption superiority. The structural behaviors of deposited nanoparticles were also analyzed by Raman spectra and disclosed the existence of tetragonal anatase and ructile segments. EDS results confirmed that the dopant of pH values of the solutions might affect the size distributions of the Fe: TiO_2 nanoparticles. The general decrement intensity was witnessed from photoluminescence outcomes.

1. Introduction

Nanoscience and nanotechnology are developing and exponentially mounting areas with large solicitations in modern technology. The nanoparticle is an interdisciplinary part of an investigation by using essential methods of different aspects like chemicals, engineering, physical and biological knowledge, and foremost to the expansion of new approaches to operating small size particles consequential in the manufacture of nanoparticles. These Nanoparticles might describe as units approximately ranging from 1 to 100 nanometers. Nanotechnology deals with the depositions, growth, and solicitations of a multiplicity of nanoparticles [1]. Nanoparticles of (Fe:TiO_2) are hopeful resources and broadly used in numerous claims because of their extremely useful and actual devices, different sensors; reagents, optoelectronic, structural and current belongings; antimicrobial, brilliant gas-sensitive, and dielectric assets; optical and electrical possessions; best chemical constancy; and the dilapidation of contamination. Because of admirable

thermal stability, extraordinary sunlight reactivity, and sensitivity, comparatively cheaper tools, iron doped titanium dioxide nanoparticles are applicable in numerous manufacturing. In addition, iron doped titanium dioxide nanoparticles are brilliant photocatalysts because of their nontoxicity, higher photo sensitivity, solid corroding power, easy obtainability, and sustainability [2, 3]. According to the meaning of the term, water repellent fabrics are those that resist water from their surface [4]. The fluoro-alkyl-silanes are the chemicals that are most frequently utilized for hydrophobization because of their extremely low surface free energy and the facile interaction of the silane clusters and the hydroxyl groups on coverings. Additionally, the hydrophobization of a perfluorinated substance [5] is responsible for the formation of the majority of superoleophobic surfaces. Wettability is among the essential features of a solid surface, as well as the contact angle has now been widely utilized to examine the wettability of a solid surface in many applications.

A great deal of interest has been generated in superhydrophobic surfaces as a result of its possible practical uses, which include anti-sticking, anticontamination, as well as self-cleaning coatings. The mechanism is comparable to the lotus effect, which occurs naturally in the environment. *Lotus* plants have extremely hydrophobic surfaces that are rough and textured, making them ideal for growing in water. When water droplets land on them, the droplets condense and, if the surface slopes sufficiently, roll off the surface into the surrounding air. As a result, even during a torrential downpour, the surfaces remain dry. Furthermore, because the droplets pick up microscopic bits of dirt as they roll down the leaves of the lotus plant, the leaves of the plant remain clean even when it is raining lightly [6]. Also known is that nanosized Fe: TiO_2 and ZnO particles are much more highly effective at absorbing and scattering UV light than conventionally sized Fe: TiO_2 and ZnO particles, and as a result, they were significantly able to block UV radiation due to their significantly greater surface area to volume ratio. A great deal of effort has been put into the application of UV bulking treatment to fabrics with the use of nanotechnology. The sol-gel process has been used to generate UV blocking treatments for fabric, which were developed by Xin and colleagues. On the surface of treated cotton fabric, a thin layer of Fe: TiO_2 nanoparticles is created, which provides good UV protection. The finish is durable and may withstand up to 50 items of washings in the washing machine. As an alternative to Fe: TiO_2, ZnO nanorods ranging in length from 10 to 50 nm were also put into the cotton fabric to give UV protection. The rods provided good ultraviolet protection [7].

In nanoparticles of iron doped titanium dioxides, the electronic arrangements, as well as the charge behaviors, are powerfully exaggerated by crystalline segment. Iron doped titanium dioxides nanoparticles can exist as anatase, rutile, and brookite phases. The structure of anatase and rutine is tetragonal, and orthorhombic is for brookite [8]. From these types, anatase is meta-stable with maximum photocatalytic movement and completely transformed to the rutile phase at a maximum temperature [9]. In another way, increases in pH value sort phase alterations, that is, amorphous to anatase, anatase to rutile. Maximum chemical constancy and fewer activities of iron doped titanium dioxides were perceived in rutile behaviors [10]. As well, some iron doped titanium dioxides have a huge magnitude of anatase, and a minor magnitude of rutile exhibitions a more sophisticated photocatalytic action than in the rutile types. Among absorption spectrum, the advantageous semiconductors for sunlight catalysis involve a bandgap analogous to the energy of that of the energy of photons of visible or ultraviolet light, containing a value below 3.5 eV. The mainstream of investigators make sure definite that in iron doped titanium dioxide, the rutile partakes an unintended bandgap of three-point one zero electron volt and a direct energy band gap of three-point zero one electron volt, and anatase has only an indirect energy bandgap 3.23 eV [11].

Nevertheless, Reddy's work [12] reports that the bandgap of anatase segment from the conspiracy for indirect conversion is quite small (2.9–2.98 eV), which commanded them, conflicting with the other scholars, to generalize that the direct conversion is more promising for iron doped titanium dioxide nanoparticles with anatase type. The reported standards in numerous literature that 2.86–3.34 electron volt for the anatase type are the modifications being qualified to deviations in the stoichiometry of the preparations, the crystal size, the impurities compositions, and the kind of electronic conversion [13]. Various techniques have been published in the literature that iron doped titanium dioxide nanoparticles were deposited by chemical-precipitation [14], the sol-gel techniques [15, 16], hydrothermal [17], and solvothermal progressions [18], combustion techniques [2], a microemulsion, mediated techniques, electro-chemical preparations, fungus-mediated preparations, and chemical vapor synthesis [19]. Works [20] reported that iron doped titanium dioxide nanoparticles were equipped through the sol-gel technique by varying reaction constraints, such as hydrolyzing agents, molar ratio, and string time. Nanocrystals of Fe: $TiO_2$with maximum surface area and varying ratios of anatase or rutile were achieved from X-ray diffraction data, prepared via sol-gel techniques. Other literature [20] also published on the synthesis of anatase Fe: TiO_2 nanocrystals found by the sol-gel technique using titanium tetra-iso-pro-peroxide in ethylene glycol leads to maximum surface area standards as well as preserved anatase per small crystal size. Sol-gel techniques are the most significant and hopeful methods working in the manufacture of nanoparticles [21]. This technique yields high crystal oxides by permitting governor in particle size, surface morphology, and phase configuration in pH values. pH values have a vital role in the creation of Fe: TiO_2 crystalline phases. Hence, the objective of this research was to study the influence of pH values on structural, optical, and morphological behaviors of deposited iron doped titanium dioxide Nanoparticles through sol-gel techniques for self-cleaning application.

2. Materials and Methodology

2.1. Chemicals Used. In preparation of iron doped titanium dioxide Nanoparticles, the chemical used as glacial acetic

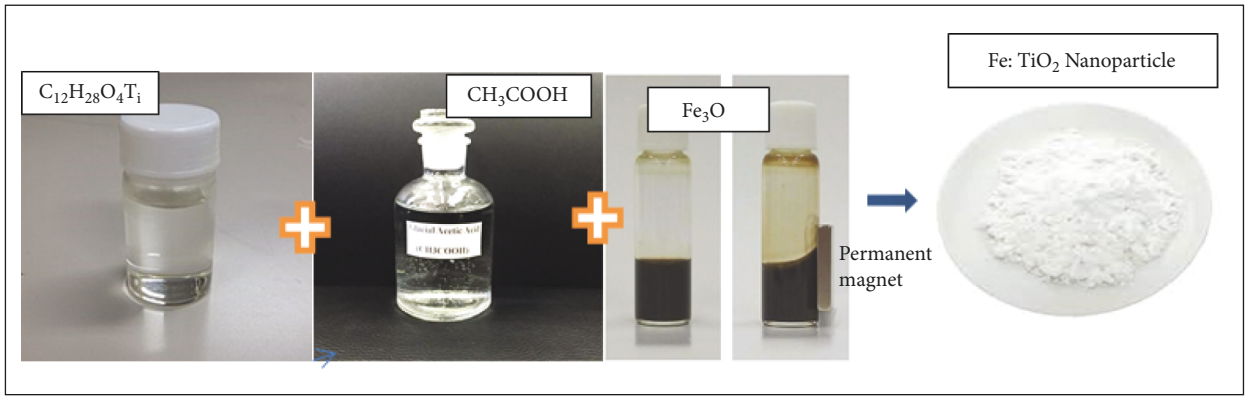

Figure 1: The procedure of material preparation.

acid (CH_3COOH) (98% LyondellBase Acetayls, LLC) and titanium (IV) iso-prop-oxide ($C_{12}H_{28}O_4Ti$) (99.9% Hebei, China) and Ferrous Oxide (Fe_3O) (98%, Zhejiang, China).

2.2. Instruments Used. Instruments used in the laboratory were magnetic stirrer, heater, thermometer, pH meter, Teflon pot, metallic pestle, and mortar auto-claves and beakers.

2.3. Sample Preparation Techniques. For the present study, Sol-gel techniques of Fe: TiO_2 nanoparticles were produced according to the process developed [22] by varying pH values of 2, 4, 5, and 6. The solution was administered by the ratio of 6Fe: TiO_2: $30CH_3COOH$: $320H_2O$. 72 ml of glacial acetic acid was slowly added to 32 ml of titanium (IV) iso-prop-oxide in a water bath at zero degrees Celsius by unceasing stirring. Then and there, 320 ml of distilled water was moderately added to the solution under stable stirring by using a magnetic stirrer, and 20 ml of ferrous Oxide was added to the solution. Ultrasonic conduct took place for 20 hr after dynamic anxiety (45 min). All over again, dynamic agitation was pragmatic for 3 hr. The mixture was decanted into a Teflon pot and located in stainless steel autoclaves. Next, step by step, iron doped titanium dioxide nanopowders were produced at 2, 4, 5, and 6 PH values, as shown in Figure 1. Lastly, the solid trials gained were ground by using a metallic pestle and mortar and kept in sample container glass.

2.4. Physical Characterizations. The consequential powders were analyzed by using instruments like X-ray diffraction, Scanning electron microscope, UV/Visible, and Fluorescence Spectroscopy. X-ray Diffraction (XRD) analysis was carried out utilizing a D8 Advance Bruker system using CuKα ($\lambda = 0.154056$ nm) radiation. The average crystalline size of produced Fe: TiO_2 Nanoparticle was determined from the peaks of XRD augmentation by using the Debye–Scherer formula [23].

$$dhkl = \frac{0.9\,\lambda}{\beta \cos\theta,} \tag{1}$$

where d_{hkl} is the average crystallite size, λ is the wavelength of the X-ray (0.15425 nm for Cu-Kα), β is the Full width at half maxima in radian, and θ is Braggs diffraction angle (? = $2d\sin\theta$) agrees to the peak position. The grain magnitude (ε), lattice constraints "a"and "c" and the distance of the space d_{hkl} aimed at anatase and ructile phase of iron doped titanium dioxide nanoparticles could be deliberated by using equations (2)–(4) [24, 25].

$$\varepsilon = \frac{\beta}{4\tan\theta}, \tag{2}$$

$$a = \sqrt{\frac{1}{3}}\ \frac{\lambda}{\mathrm{Sin}\,\theta}\mathrm{c} = \frac{\lambda}{\mathrm{Sin}\,\theta}, \tag{3}$$

$$\mathrm{dhkl} = \frac{\mathrm{ac}}{2}\sqrt{\frac{3}{\mathrm{c}^2\left(\mathrm{h}^2 + \mathrm{hk} + \mathrm{k}^2\right) + 3\left((\mathrm{al})^2 |4\right)}}. \tag{4}$$

The unit cell volume (V) and O-Ti-O bond length (L) are given by [26]

$$V = 0.866\mathrm{a}^3 cl = \frac{\mathrm{a}^3}{3} + \left(\frac{1}{2} - \mathrm{z}\right)^2 \mathrm{c}^2 Z = \frac{\mathrm{a}^2}{3\mathrm{c}^2} + \frac{1}{4}. \tag{5}$$

The surface morphology, as well as the nanostructure of the occasioning iron doped titanium dioxide (Fe: TiO_2) Nanoparticles, was analyzed with the help of a scanning electron microscope. The structural characteristics of synthesized Fe: TiO_2 powders were examined by a Raman shift (RAM, HR Spectrometer). Optical absorption spectra were recorded with a Perkin–Elmer Lambda-19 spectrophotometer in the 300–800 nm range. The bandgap energy of Fe: TiO_2NPs is calculated using equation (6) [1].

$$\mathrm{E} = \frac{\mathrm{hc}}{\lambda}, \tag{6}$$

where h is plank's constant ($h = 6.626\mathrm{x}10^{-34}$Js) C is the speed of light ($\mathrm{c} = 3 \times 10^8$ m/s, and λ is the wavelength. Photoluminescence (PL) quantities were accomplished at normal temperature by using an instrument called fluorescence spectrophotometer (LS-45) with an excitation wavelength of 260 Nanometer.

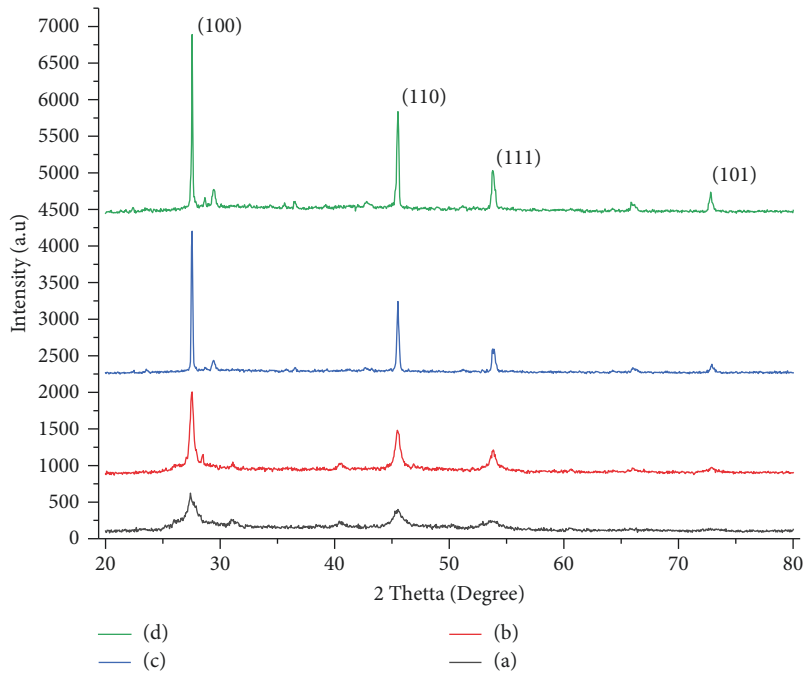

Figure 2: XRD graph of prepared iron doped titanium dioxide at different pH values of (a) pH = 2, (b) pH = 4, (c) pH = 5, and (d) pH = 6.

Table 1: The full width at half maxima (FWHM), average particle size and average crystal values of Fe: TiO_2 NPs at different pH values (2, 4, 5, and 6)

Sample	pH value	2Theta (Degree)	Theta (θ(degree)	FWHM (Radian)	Crystal Size (nm)
1	2	27.29508	13.64	0.11341	72
2	4	45.31616	22.65	0.11153	77
3	5	53.44262	26.72	0.11325	78
4	6	66.22951	33.11	0.11406	83

3. Results and Discussion

3.1. Structural Analysis of Fe: TiO2 Nanoparticles. Figure 2 expresses X-ray diffraction spectra of the produced iron doped titanium dioxide nanoparticles following sol-gel techniques at pH values of 2, 4, 5, and 6, which contracts the existence of anatase and ructile phase of iron doped titanium dioxide liable on pH values. The spectrum displays well-defined peaks of iron doped titanium dioxide nanoparticles. Nearby six analytical peaks were perceived at $2\theta = 27.295^{o}$, 45.31^{o}, $53.44^{o,}$ and $66.22^{o,}$ and their corresponding reflection of miller indices (100), (110), (111), and (101), respectively, for these pH values. Phase transformation is observed from anatase to rutine as the pH value increases from two to six. In other ways, anatase phases were evidently performed at 2 and 4 while ructile phases were observed at 5 and 6. All diffraction angles were well indexed to ructile and anatase configuration, which is nicely in agreement with that of reported works [27]. The strength peaks of deposited micromaterials become shriller with increasing pH values because of an increase in crystal size and crystalline structure.

The crystal sizes of prepared iron doped titanium dioxide nanoparticles were evaluated by using a Debye–Scherer equation with equation (1) depending on the deflection angle and full width at half-maximum (FWHM) of the peaks as described in Table 1 below. The average crystal size of prepared Fe: TiO_2 nanoparticles at pH values of 2, 4, 5, and 6 are 77.5, and the crystal sizes of Fe: TiO_2 nanoparticle were increased with pH value increased for both anatase and ructile phase, which is in good agreement with the result reported [28]. Additionally, Full Width at Half Maxima (FWHM), as well as middling grain size of produced Fe: TiO_2 Nanoparticles, declined with increasing pH value from 2 to 6. The crystal sizes are gained from Debye–Scherer's formula.

The influence of pH value on prepared titanium nanoparticles was evaluated by using equations (3)–(5). The lattice constraints of Fe: TiO_2 Nanoparticles were increased with pH value. Lattice constraints of prepared nanoparticles had agreed with that of TiO_2 previously [15]. The pH rate leads to perfection in crystalline size, deflection strength, oxygen–titanium–oxygen bond length, and volume of the unit cell.

3.2. Scanning Electron Microscope (SEM) Characterization of Fe: TiO_2 Nanoparticles. Figure 3 shows the morphology of deposited iron doped titanium dioxide nanoparticles samples at pH values of 2, 4, 5, and 6 using a scanning electron

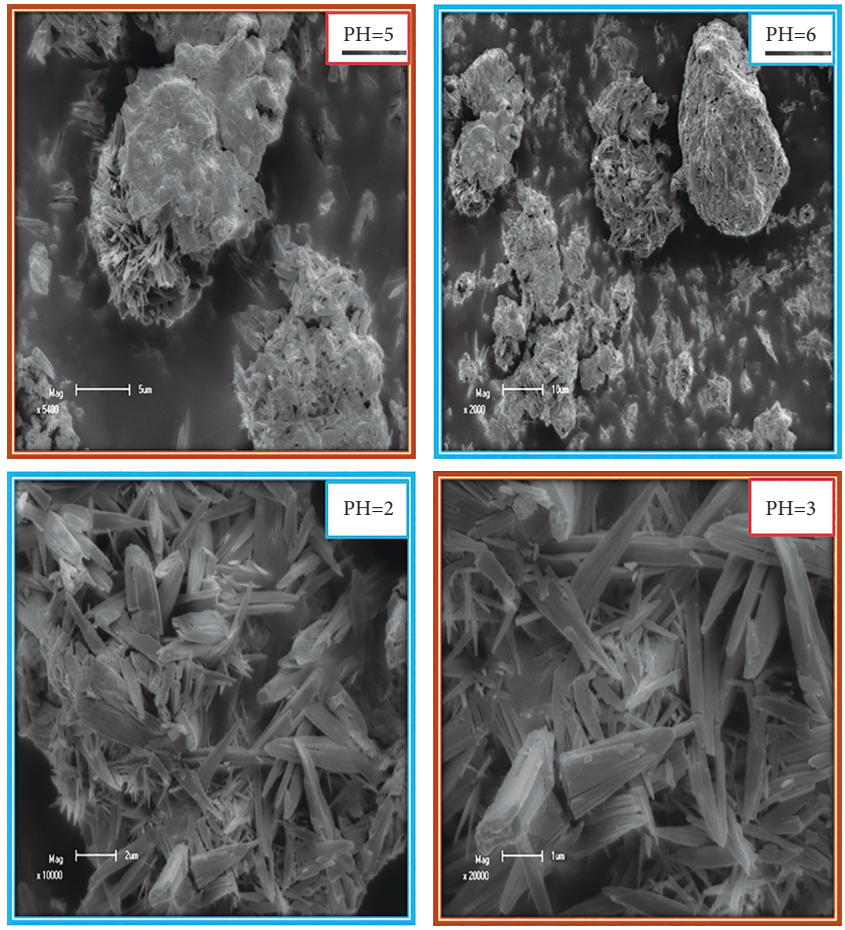

Figure 3: SEM images of synthesized Fe : TiO_2NPs at PH values of 2, 4, 5, and 6.

microscope (SEM) (Model CamScan MV2300). Homogenously disseminated cylindrical structure iron doped titanium dioxide NPs were perceived from Scanning electron microscope (SEM) micrographs. As shown in Figure 2 the middling size of deposited iron doped titanium dioxide nanoparticles was rising with pH tenets. SEM images at pH 2 and pH 3 are somewhat similar to fixed wood images as well as micrographs at pH 5 and 6 are also similar, and the image is like broken rocks. An accumulation of prepared iron doped titanium dioxide nanoparticles happened throughout pH values because of in height surface energy of nanoparticles.

3.3. Optical Characterization of Fe: TiO_2 NPs. The optical analysis of Fe TiO_2 nanoparticles using UV–Vis spectrophotometer (Schimadzu UV-1800) in the wavelength range of 250–700 nm. Figure 4 displays the absorbance spectrum of samples prepared at different pH values. The highly transparent nanopowders are seen in the visible region. The observed redshift towards higher wavelengths with a rising pH value is owing to an increase in particle size, as evidenced by XRD and SEM pictures [16]. Because oxygen vacancies form deep levels in the bandgap, the existence of oxygen vacancies at greater pH values may also be related to the aforesaid effect [29].

The energy band gap values of synthesized Fe : TiO_2 NPs are obtained by using the equation. UV/Visible studies show that the energy band gap decreases with increasing pH values of Fe : TiO_2NPs, corresponding to a redshift of the optical absorption edge [30]. This is due to an increase in pH value and a lowers inter-atomic spacing. It is noteworthy here that values of energy band gap obtained are lesser in comparison to the energy band gap 3.1 eV for pure anatase, 3 eV for rutile phase, and the data reported for the mixed-phase Fe : TiO_2 nanopowders exhibiting as a capable candidate for self-cleaning application [31].

3.4. Photoluminescence (PL) Spectral Analysis of Fe: TiO2 NPs. The optical behaviors of deposited Nanoparticles are also studied by using photoluminescence. Photoluminescence spectra of the prepared specimens were documented at room temperature in the range of wavelength between 400 nm and 700 nm, as depicted in Figure 5. The overall photoluminescence intensity decreases as the pH value increases from 2 to 6. The highest PL intensity at pH values 4 and 5 is mainly due to self-trapped exciton recombination, generated from oxygen vacancy and particle size which is known as defect centers [32]. The PL intensity decreases steadily with the increasing pH value from 2 to 6. The behavior of increment and decrement behavior is mainly due to isolated

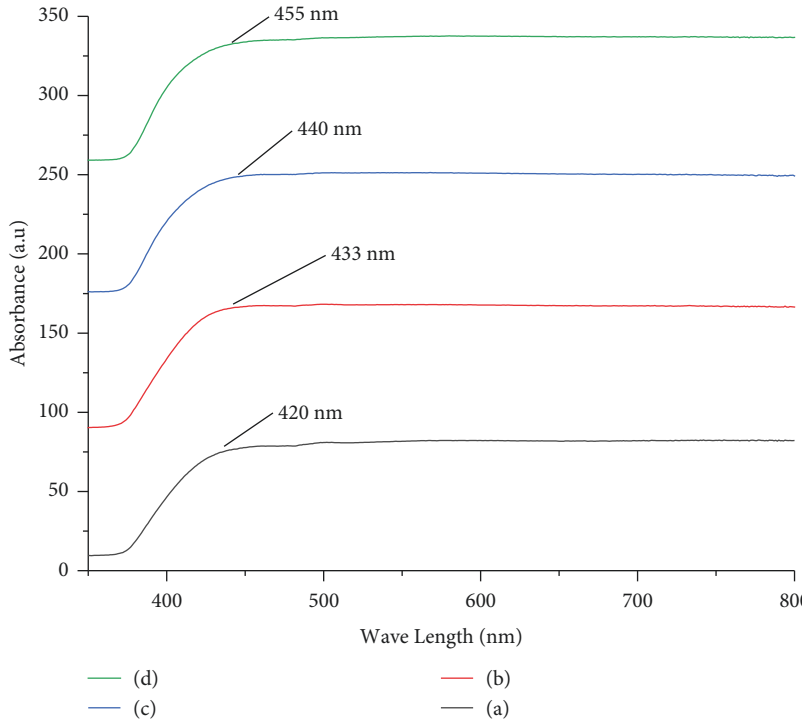

Figure 4: Absorbance spectra of Fe TiO_2NPs at PH value of (a) PH = 2, (b) pH = 4, (c) pH = 5, and (d) pH = 6.

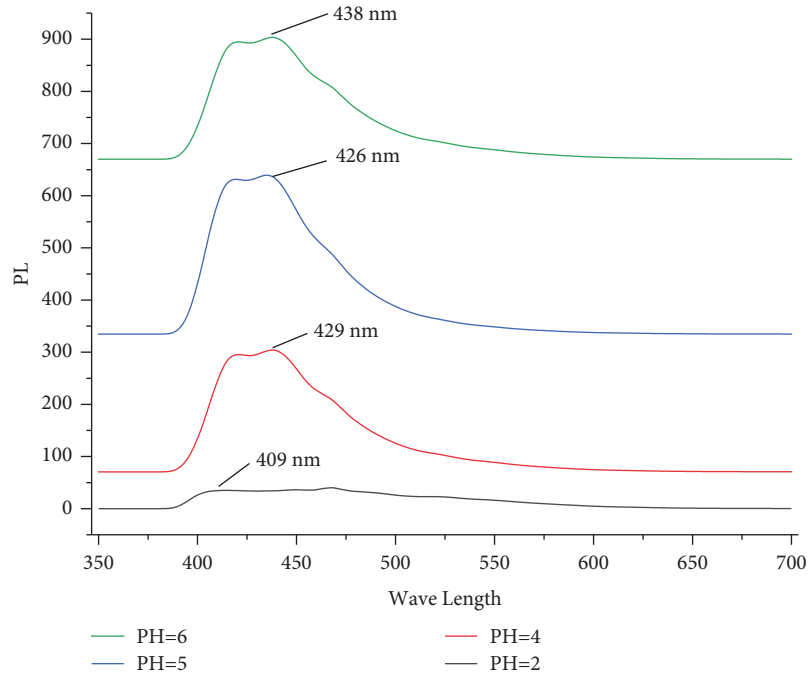

Figure 5: Photoluminescence spectra of prepared Fe TiO_2 Nanoparticles at pH values of 2, 4, 5, and 6. Energy-dispersive X-ray spectroscopy (EDS) characterization.

phases of anatase and rutile. As shown in Figure 5, Due to the increment of pH value, a new radioactive transition occurs, which leads to a new PL peak at the rutile phase [33–35]. The Photoluminescence strength of the peaks increases as the pH increases; this result shows that oxygen vacancies appear slowly with pH value. An anatase phase is perceived at pH = 2 and pH = 4 whereas the rutile phase looks at maximum pH value. The concentration of anatase and rutine peaks declines and then gradually appears for higher pH values. The growth of other peaks around the

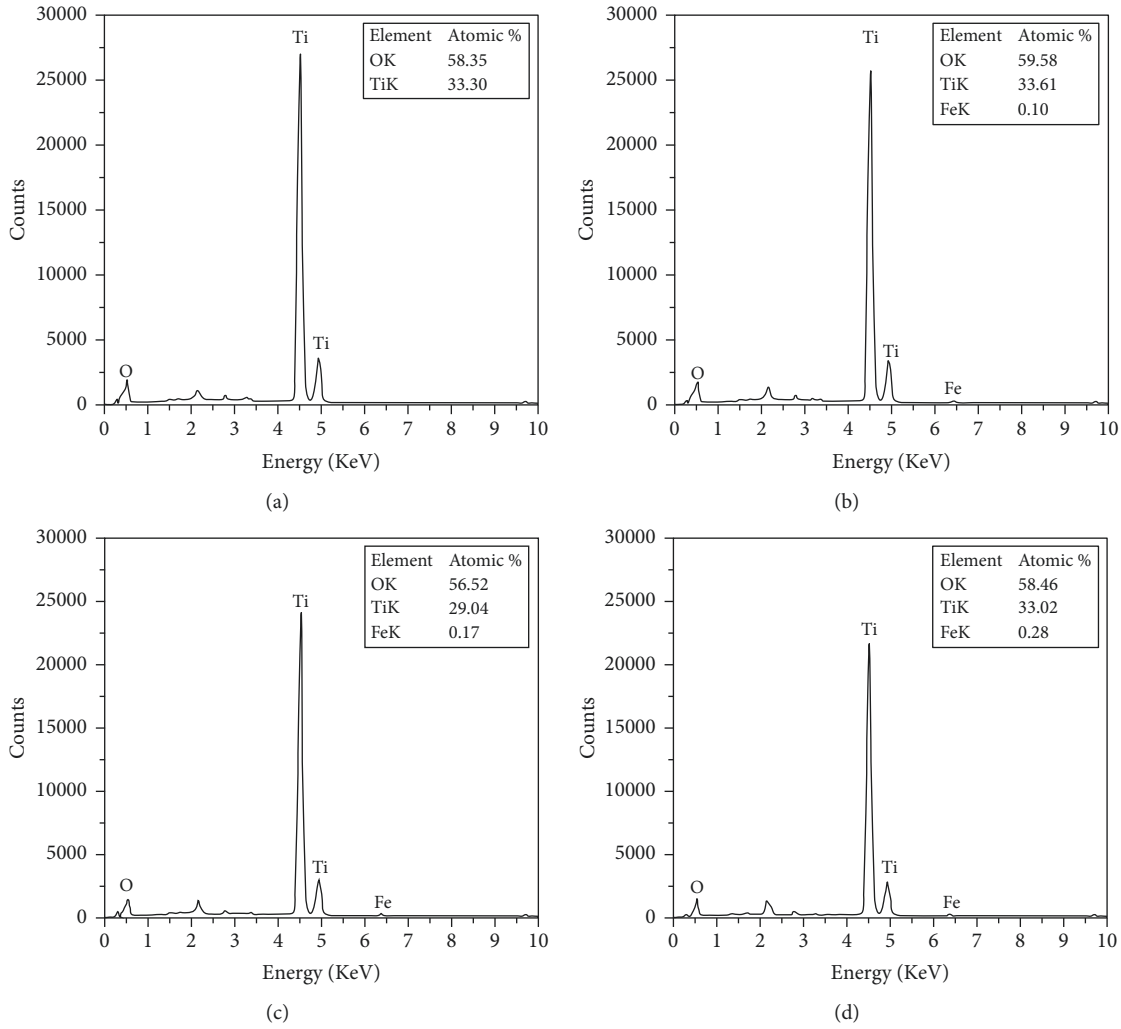

Figure 6: EDS patterns of Fe TiO_2 Nanoparticles at different pH values (a) pH = 2, (b) pH = 4, (c) pH = 5, and (d) pH = 6.

438 nm peak may indicate the existence of other voids inside the bandgap and narrow traps mainly basis on the surface morphology dissemination nanostructures [36].

EDS measurements were performed for all samples in a Hitachi TM3000 Tabletop microscope at the NTNU nano lab. The impact of iron ions doping on the chemical configuration was studied by energy-dispersive X-ray spectroscopy (EDS). Figure 6 displays the energy-dispersive X-ray spectroscopy (EDS) patterns of Fe : TiO_2 Nanoparticles at different pH values, varied as 2, 4, 5, and 6. The chemical configuration of four EDS arrays (Figures 4(a)–4(d)) was calculated, and it is initiated that the chemical elemental contents of oxygen and titanium have not altered significantly. At similar times, we can find that the elemental chemical components of iron were gradually growing. The chemical elemental contents of C are not displayed; they can arise from showing resin. Thus, EDS results in supplementary confirmed that the dopant of pH values of the solutions might affect the size distributions of the Nanoparticles. Figure 6 displays the sono-catalytic activities of Fe doped TiO_2 nanoparticles with different Fe^{3+} ion contents. It can be seen that the Fe dopant content has no noticeable influence on the degradation rate under our study circumstances. So, we chose pH = 5 as the best quantity of iron for TiO_2 due to its larger specific surface area [37].

4. Conclusions

Iron doped titanium dioxide nanoparticles with chemical formula Fe TiO_2 were produced through sol-gel technique from (CH_3COOH) and titanium (IV) iso-prop-oxide ($C_{12}H_{28}O_4Ti$) at pH values of 2, 4, 5, and 6. The prepared nanoparticles were analyzed by X-ray diffraction, scanning electron microscope, UV/Visible spectroscopy, and photoluminescence and were perceived from XRD data and revealed that there was the formation of anatase and rutine phase with hexagonal structure. A pH value gives the alteration of phases from anatase to rutine. Uniformly distributed hexagonal shapes of nanoparticles were shown from scanning electron microscope micrograph and increased in size with increasing pH values from 2 to 6. Extremely transparent nanopowders are witnessed in the visible region from UV/Visible and a slight red shift in the UV/Visible peaks towards higher wavelength as rising pH value. The PL

intensity of the peaks increases as the pH value increases. EDS results confirmed that the dopant of pH values of the solutions might affect the size distributions of the Fe TiO_2 Nanoparticles. This result indicates that oxygen vacancies appeared slowly with pH value; all results show Fe TiO_2 nanoparticles are promising for self-cleaning materials [38–41].

Data Availability

The data used to support the findings of this study are included in the article.

Disclosure

This study was performed as a part of the employment of the authors, Dambi Dollo University,Ethiopia.

Conflicts of Interest

The authors declare that there are no conflicts of interest regarding the publication of this article.

References

[1] S. Dai, Y. Wu, T. Sakai, Z. Du, H. Sakai, and M. Abe, "Preparation of highly crystalline TiO2 nanostructures by acid-assisted hydrothermal treatment of hexagonal-structured nanocrystalline titania/cetyltrimethyammonium bromide nanoskeleton," *Nanoscale Research Letters*, vol. 5, no. 11, pp. 1829–1835, 2010.

[2] K. Vijayalakshmi and V. Rajendran, "Synthesis and characterization of nano-Fe: TiO2 via different methods," *Archives of Applied Science Research*, vol. 4, pp. 1183–1190, 2012.

[3] J. Lin, M. Guo, C. T. Yip et al., "High temperature crystallization of free-standing anatase TiO2Nanotube membranes for high efficiency dye-sensitized solar cells," *Advanced Functional Materials*, vol. 23, no. 47, pp. 5952–5960, 2013.

[4] K. Shankar, J. I. Basham, N. K. Allam et al., "Recent advances in the use of TiO2 nanotube and nanowire arrays for oxidative photoelectrochemistry," *Journal of Physical Chemistry C*, vol. 113, no. 16, pp. 6327–6359, 2009.

[5] N. K. Allam and M. A. Ei-Sayed, "Effective photocatalytic properties of N-doped Iron doped Titanium dioxide nanotube arrays prepared by anodization," *Journal of Physical Chemistry C*, vol. 112, p. 12687, 2010.

[6] H. I. Hsiang and S. C. Lin, "Effects of aging on the phase transformation and sintering properties of TiO2 gels," *Materials Science and Engineering A*, vol. 380, no. 1-2, pp. 67–72, 2004.

[7] P. Roy, S. Berger, and P. Schmuki, "TiO2 nanotubes: synthesis and applications," *Angewandte Chemie International Edition*, vol. 50, no. 13, pp. 2904–2939, 2011.

[8] J. K. Tsai, W. D. Hsu, T. C. Wu, T. H. Meen, and W. J. Chong, "Effect of compressed Fe: TiO2 nanoparticle thin film thickness on the performance of dye-sensitized solar cells," *Nanoscale Research Letters*, vol. 8, pp. 79–85, 2013.

[9] G. K. Mor, O. K. Varghese, M. Paulose, K. Shankar, and C. A. Grimes, "A review on highly ordered, vertically oriented TiO2 nanotube arrays: fabrication, material properties, and solar energy applications," *Solar Energy Materials and Solar Cells*, vol. 90, no. 14, pp. 2011–2075, 2006.

[10] S. Kathirvel, C. Su, C. Y. Yang, Y. J. Shiao, B. R. Chen, and W. R. Li, "The growth of TiO2 nanotubes from sputter-deposited Ti film on transparent conducting glass for photovoltaic applications," *Vacuum*, vol. 118, pp. 17–25, 2015.

[11] V. Galstyan, E. Comini, G. Faglia, and G. Sberveglieri, "TiO2 nanotubes: recent advances in synthesis and gas sensing properties," *Sensors*, vol. 13, no. 11, pp. 14813–14838, 2013.

[12] Y. J. Park, J. M. Ha, G. Ali, V. Kim, Y. Addad, and S. O. Cho, "Controlled fabrication of nanoporous oxide layers on zircaloy by anodization," *Nanoscale Research Letters*, vol. 10, no. 1, p. 377, 2015.

[13] Y. Li, H. Yu, C. Zhang et al., "Effect of water and annealing temperature of anodized TiO2 nanotubes on hydrogen production in photoelectrochemical cell," *Electrochimica Acta*, vol. 107, pp. 313–319, 2013.

[14] O. Khatim, M. Amamra, K. Chhor et al., "Amorphous-anatase phase transition in single immobilized TiO2 nanoparticles," *Chemical Physics Letters*, vol. 558, pp. 53–56, 2013.

[15] D. Yoo, I. Kim, S. Kim, C. H. Hahn, C. Lee, and S. Cho, "Effects of annealing temperature and method on structural and optical properties of TiO2 films prepared by RF magnetron sputtering at room temperature," *Applied Surface Science*, vol. 253, no. 8, pp. 3888–3892, 2007.

[16] C. V. R. Vasantkumar and A. Mansingh, "Structural evolution and optical properties of Fe: TiO2 thin films prepared by thermal oxidation of sputtered Ti films," *Seventh IEEE International Symposium on Application of Ferroelectrics*, IEEE, vol. 88, pp. 713–716, 1990.

[17] V. Chaudhary, A. Srivastava, and J. Kumar, "On the sol-gel synthesis and characterization of titanium oxide nanoparticles," *Materials Research Society Symposia Proceedings*, vol. 1352, p. 759, 2011.

[18] A. Cesnovar, P. Paunovic, A. Grozdanov, and E. Fidanchevska, "Preparation of nano-crystalline Fe: TiO2 by sol-gel method using titanium tetraisopropoxide (TTIP)," *Adv. Nat. Sci. Theory Appl.*vol. 1, pp. 133–142, 2012.

[19] S. Dai, Y. Wu, T. Sakai, Z. Du, H. Sakai, and M. Abe, "Preparation of highly crystalline Fe: TiO2 nanostructures by acid-assisted hydrothermal treatment of hexagonal-structured nanocrystalline titania/cetyltrimethyammonium bromide nanoskeleton," *Nanoscale Research Letters*, vol. 11, pp. 1829–1850, 2017.

[20] H. Kominami, J. Kato, Y. Takada et al., "Novel synthesis of microcrystalline titanium (IV) oxide having high thermal stability and ultra-high photocatalytic activity, thermal decomposition of titanium(IV) alkoxide in organic solvents," *Catalysis Letters*, vol. 46, no. 3/4, pp. 235–240, 1997.

[21] H. Li, T. Xie, H. Wang, and Z. Du, "A facile solution-phase synthesis of high quality water soluble anatase Fe: TiO2 nanocrystals," *Journal of Colloid and Interface Science*, vol. 314, pp. 337–340, 2007.

[22] A. L. Linsebigler, G. Lu, and J. T. Yates, "Photocatalysis on TiO2 surfaces: principles, mechanisms, and selected results," *Chemical Reviews*, vol. 95, no. 3, pp. 735–758, 1995.

[23] K. Nagaveni, G. Sivalingam, M. S. Hegde, and G. Madras, "Solar photocatalytic degradation of dyes, high activity of combustion synthesized nano Fe: TiO2," *Applied Catalysis B: Environmental*, vol. 48, pp. 83–93, 2003.

[24] S. Pavasupree, J. Jitputti, S. Ngamsinlapasathian, and S. Yoshikawa, "Hydrothermal synthesis, characterization, photocatalytic activity and dye-sensitized solar cell performance of mesoporous anatase TiO2 nanopowders," *Materials Research Bulletin*, vol. 43, no. 1, pp. 149–157, 2008.

[25] C. Weiwei, Y. Hui, and G. Xingzhong, "A facile synthesis of nanocrystalline spherical Fe: TiO2 particles and its photoluminescent properties," *Procedia Engineering*, vol. 94, pp. 71–75, 2014.

[26] S. Bakardjieva, J. Šubrt, V. Štengl, M. J. Dianez, and M. J. Sayagues, "Photoactivity of anatase-rutile TiO2 nanocrystalline mixtures obtained by heat treatment of homogeneously precipitated anatase," *Applied Catalysis B: Environmental*, vol. 58, no. 3-4, pp. 193–202, 2005.

[27] A. K. Tripathi, M. K. Singh, M. C. Mathpal, S. K. Mishra, and A. Agarwal, "Study of structural transformation in TiO2 nanoparticles and its optical properties," *Journal of Alloys and Compounds*, vol. 549, pp. 114–120, 2013.

[28] A. Zareen, S. Ali, and M. Irfan, "The effect of PH values on phase and optical properties of Fe: TiO2 nanoparticles for solar cell applications," *ESJ*, vol. 2, pp. 447–450, 2014.

[29] S. Pawar, M. Chougule, S. Patil et al., "Fabrication of nanocrystalline TiO₂ thin film ammonia vapor sensor," *Journal of Sensor Technology*, vol. 01, no. 01, pp. 9–16, 2011.

[30] S. G. Pawar, M. A. Chougule, P. R. Godse et al., "Effect of annealing on structure, morphology, electrical and optical properties of nanocrystalline Fe: TiO2 thin films," *J. Nano Electron Phys*, vol. 3, pp. 185–192, 2011.

[31] H. C. Choi, Y. M. Jung, and S. B. Kim, "Size effects in the Raman spectra of TiO2 nanoparticles," *Vibrational Spectroscopy*, vol. 37, no. 1, pp. 33–38, 2005.

[32] C. Y. Xu, P. X. Zhang, and L. Yan, "Blue shift of Raman peak from coated TiO2 nanoparticles," *Journal of Raman Spectroscopy*, vol. 32, no. 10, pp. 862–865, 2001.

[33] C. Rath, P. Mohanty, A. C. Pandey, and N. C. Mishra, "Oxygen vacancy induced structural phase transformation in Fe: TiO2 nanoparticles," *Journal of Physics D: Applied Physics*, vol. 42, P. 205101, 2009.

[34] H. Zhang and J. F. Banfield, "New kinetic model for the nanocrystalline anatase-to-rutile transformation revealing rate dependence on number of particles," *American Mineralogist*, vol. 84, no. 4, pp. 528–535, 1999.

[35] M. C. Mathpal, A. K. Tripathi, M. K. Singh, S. P. Gairola, S. N. Pandey, and A. Agarwal, "Effect of annealing temperature on Raman spectra of TiO2 nanoparticles," *Chemical Physics Letters*, vol. 555, pp. 182–186, 2013.

[36] C. K. Chung, M. W. Liao, and C. W. Lai, "Effects of oxygen flow ratios and annealing temperatures on Raman and photoluminescence of titanium oxide thin films deposited by reactive magnetron sputtering," *Thin Solid Films*, vol. 518, no. 5, pp. 1415–1418, 2009.

[37] R. H. Waghchaure, P. B. Koli, V. A. Adole, T. B. Pawar, and B. S. Jagdale, "Transition metals Fe3+, Ni2+ modified titanium dioxide (TiO2) film sensors fabricated by CPT method to sense some toxic environmental pollutant gases," *Journal of the Indian Chemical Society*, vol. 98, no. 9, p. 100126, 2021.

[38] T. Bezrodna, T. Gavrilko, G. Puchkovska, V. Shimanovska, J. Baran, and M. Marchewka, "Spectroscopic study of TiO2 (rutile)-benzophenone heterogeneous systems," *Journal of Molecular Structure*, vol. 614, no. 1-3, pp. 315–324, 2002.

[39] T. Ohsaka, "Temperature dependence of the Raman spectrum in anatase TiO2," *Journal of the Physical Society of Japan*, vol. 48, no. 5, pp. 1661–1668, 1980.

[40] I. Sta, M. Jlassi, M. Hajji et al., "Structural and optical properties of TiO2 thin films prepared by spin coating," *Journal of Sol-Gel Science and Technology*, vol. 72, no. 2, pp. 421–427, 2014.

[41] M. C. Mathpal, A. K. Tripathi, M. K. Singh, S. P. Gairola, and S. N. Pandey, "Effect of PH value on Raman spectra of Fe: TiO2 nanoparticles," *Chemical Physics Letters*, vol. 500, pp. 82–112, 2011.